Highly Reversible Positive-Valence Conversion of Sulfur Chemistry for High-Voltage Zinc–Sulfur Batteries

Chen, Ze; Huang, Zhaodong; Zhu, Jiaxiong; Li, Dedi; Chen, Ao; Wei, Zhiquan; Wang, Yiqiao; Li, Nan; Zhi, Chunyi

Published in:
Advanced Materials

Published: 25/07/2024

Document Version:
Final Published version, also known as Publisher's PDF, Publisher's Final version or Version of Record

Published version (DOI):
10.1002/adma.202402898

Publication details:
Chen, Z., Huang, Z., Zhu, J., Li, D., Chen, A., Wei, Z., Wang, Y., Li, N., & Zhi, C. (2024). Highly Reversible Positive-Valence Conversion of Sulfur Chemistry for High-Voltage Zinc–Sulfur Batteries. *Advanced Materials*, *36*(30), Article 2402898. https://doi.org/10.1002/adma.202402898

ADVANCED MATERIALS
www.advmat.de

Highly Reversible Positive-Valence Conversion of Sulfur Chemistry for High-Voltage Zinc–Sulfur Batteries

Ze Chen, Zhaodong Huang, Jiaxiong Zhu, Dedi Li, Ao Chen, Zhiquan Wei, Yiqiao Wang, Nan Li, and Chunyi Zhi**

Sulfur is a promising conversion-type cathode for zinc batteries (ZBs) due to its high discharge capacity and cost-effectiveness. However, the redox conversion of multivalent S in ZBs is still limited, only having achieved S^0/S^{2-} redox conversion with low discharge voltage and poor reversibility. This study presents significant progress by demonstrating, for the first time, the reversible S^{2-}/S^{4+} redox behavior in ZBs with up to six-electron transfer (with an achieved discharge capacity of ≈1284 mAh g^{-1}) using a highly concentrated ClO_4^--containing electrolyte. The developed succinonitrile–$Zn(ClO_4)_2$ eutectic electrolyte stabilizes the positive-valence S compound and contributes to an ultra-low polarization voltage. Notably, the achieved flat discharge plateaus demonstrate the highest operation voltage (1.54 V) achieved to date in Zn||S batteries. Furthermore, the high-voltage Zn||S battery exhibits remarkable conversion dynamics, excellent cycling performance (85.7% capacity retention after 500 cycles), high efficiency (98.4%), and energy density (527 Wh kg_S^{-1}). This strategy of positive-valence conversion of sulfur represents a significant advancement in understanding sulfur chemistry in batteries and holds promise for future high-voltage sulfur-based batteries.

1. Introduction

Aqueous rechargeable zinc batteries (ZBs) have emerged as a promising candidate for safe and high-energy storage devices.[1–3] Despite significant progress in improving the electrochemical performance and stability of anodes, practical applications of ZBs are still limited by the lack of high-energy and reversible cathodes, which restricts the scalability and reliability of ZBs.[4–7] For instance, intercalation-type Prussian blue analogs (PBA) deliver a high output voltage (above 1.7 V) but are limited by the low capacity;[8] V_2O_5 has a high discharge capacity but operates at a low voltage of 0.8 V.[9] Besides, these intercalation-type cathodes undergo inevitable dissolution and structural collapse during cycling.[10,11] Thus, developing cathode materials that can fulfill requirements of high capacity, high discharge voltage, and good cycling performance remains a significant challenge.

Conversion-type sulfur cathode is the potential to offer high capacity (theoretical capacity of 1675 mAh g^{-1} based on two-electrons transfer) without structure collapse during cycling.[12–14] However, sulfur-cathode-based ZBs only demonstrate a low discharge voltage of 0.47 V (**Figure 1a**), corresponding to sulfur reduction (S^0 to S^{2-}). The capacity shows a fast decay during cycling, typically attributing to the generation of zinc sulfide (ZnS) products (Figure 1b).[15] The ultralow solubility of ZnS in water exacerbates the irreversibility of S^0/S^{2-} redox in aqueous Zn||S batteries compared to other metal–sulfur batteries (Figure 1c).[16] Various strategies have been developed to enhance sulfur conversion kinetics in ZBs, including the incorporation of redox catalysts into cathodes[17,18] and the addition of redox mediators into electrolytes.[15,19,20] Despite these efforts, the discharge voltage is fundamentally limited by the low electrochemical potential of sulfur reduction (S^0 to S^{2-}), and the presence of inert ZnS products continues to pose a major challenge for achieving highly reversible aqueous Zn||S batteries.

Although sulfur element exhibits a multivalent nature (−2, 0, +2, +4, and +6), achieving electrochemical oxidation of sulfur to a positive valence in Zn||S batteries has not been successful. Though it is possible to charge the sulfur electrode to achieve the positive-valence S by applying overpotential, positive-valence chalcogens are prone to dissolution or decomposition in aqueous or organic solutions, resulting in the consumption of active materials during electrochemical cycling.[21] Commonly used anions in aqueous batteries, such as bis(trifluoromethyl) sulfonate (OTF^-), sulfate (SO_4^{2-}), and di(bis(trifluoromethylsulfonyl)imide) ($TFSI^-$), are weak

Z. Chen, J. Zhu, D. Li, A. Chen, Z. Wei, Y. Wang, N. Li, C. Zhi
Department of Materials Science and Engineering
City University of Hong Kong
83 Tat Chee Avenue, Kowloon, Hong Kong 999077, China
E-mail: nanli75@cityu.edu.hk; cy.zhi@cityu.edu.hk
Z. Huang, C. Zhi
Hong Kong Center for Cerebro-Cardiovascular Health Engineering (COCHE)
Shatin, New Territories, Hong Kong 999077, China

The ORCID identification number(s) for the author(s) of this article can be found under https://doi.org/10.1002/adma.202402898

DOI: 10.1002/adma.202402898

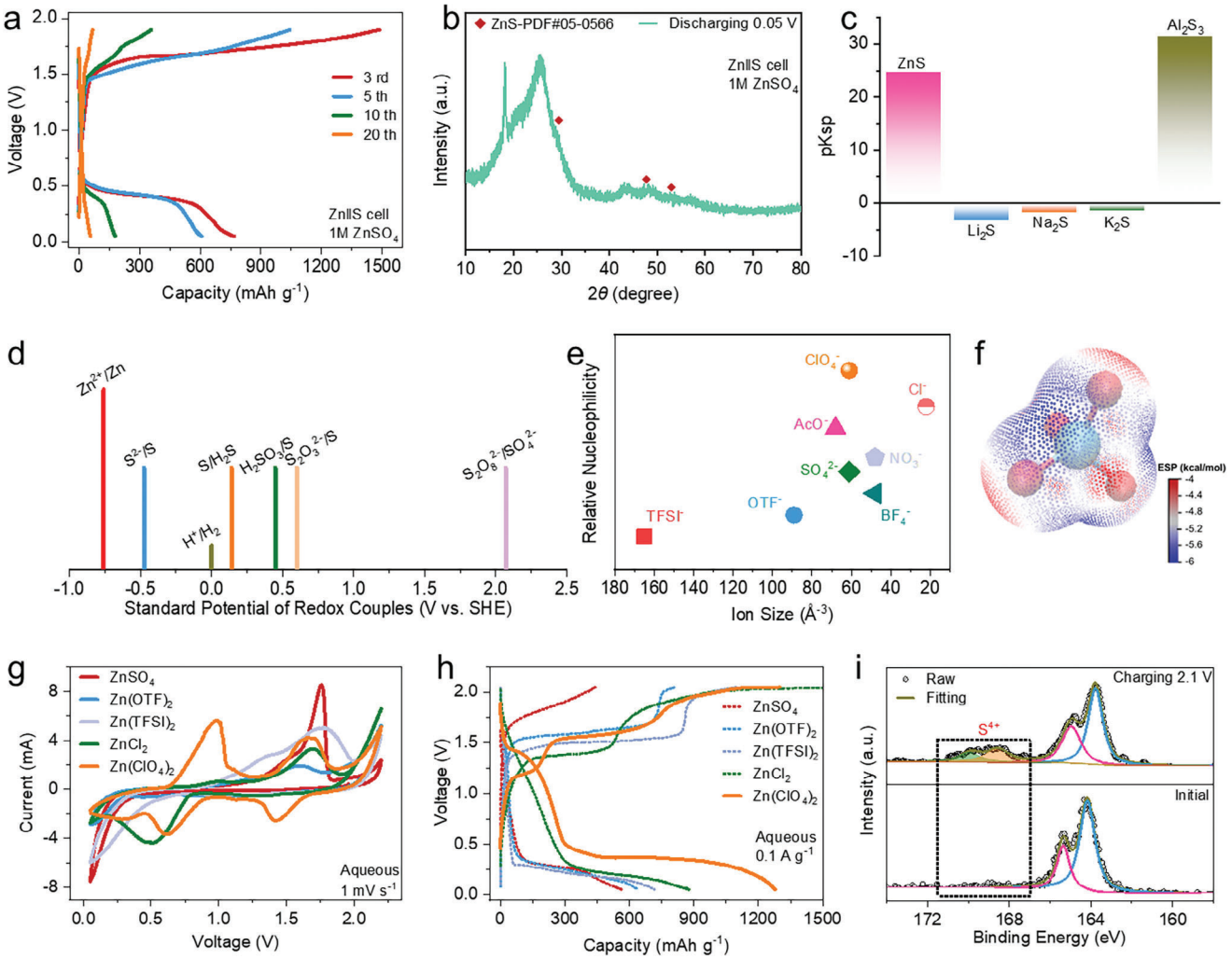

Figure 1. Strategy for activating multivalence conversion of sulfur cathode in Zn||S cells. a) GCD curves of the Zn||S cell with 1 M $ZnSO_4$ aqueous electrolyte. b) XRD patterns of sulfur cathode at initial state and 0.05 V discharging state. c) The solubility product constants (K_{sp}) of typical metal sulfide (pK_{sp} is the negative logarithm of K_{sp}). d) Standard potentials of sulfur-based redox couples (the different heights of the colored bars are only for easy labeling). e) Comparison of anion size and nucleophilicity. f) ESP mapping of ClO_4^- anion. g) CV curves of Zn||S cells with different electrolytes scanned at 1 mV s^{-1}. h) GCD curves of Zn||S cells with different electrolytes at 0.1 A g^{-1}. i) XPS spectra of sulfur cathode at initial state and 2.1 V charging state.

reductants and cannot effectively stabilize positive-valence S due to their limited nucleophilicity.[22,23] In addition, this process requires high-voltage charging,[24,25] which often leads to electrolyte decomposition and consequently poor reversibility.[22,26,27] Thus, to enable successful sulfur oxidation for the fabrication of high-energy and reversible Zn||S batteries, a stable electrolyte containing anions with strong nucleophilicity is highly desired.[25,28]

Herein, we adopt a highly concentrated $Zn(ClO_4)_2$ electrolyte (8 M $Zn(ClO_4)_2$) to achieve multivalence conversion of the sulfur cathode in Zn||S batteries, which involves an unprecedented six-electron transfer process (S^{2-}/S^{4+} redox conversion). A succinonitrile (SN)-based eutectic electrolyte is further developed to effectively suppress the dissolution of positive-valence S compounds, leading to enhanced conversion activity and cycling stability. Notably, the resulting ZBs demonstrate the highest operation voltage (1.54 V) achieved to date in Zn||S batteries. By adjusting the operating voltage window, remarkable rate performance and cycling performance are achieved in our high-voltage Zn||S battery, which is superior to common aqueous ZBs. Our work provides new insights into the design of high-voltage and reversible Zn||S batteries by enhancing multivalence conversion of sulfur chemistry.

2. Results and Discussion

2.1. Activation of Electrochemical Sulfur Oxidation

Conventional Zn||S cells with electrochemical sulfur reduction (following the S^0 to S^{2-} reaction pathway) suffer from low output voltage, low energy efficiency, and poor reversibility.[20,29] Designing electrochemically stable electrolytes that can alter reaction pathways to achieve sulfur oxidation (Figure 1d) is a

promising approach for enhancing the electrochemical performance of Zn||S cells.[24,25] It is worth noting that anions with higher nucleophilicity are beneficial for stabilizing positive-valence S, while smaller anions can facilitate ion diffusion within bulk sulfur, leading to faster conversion kinetics in sulfur-based cells.[22,30] Following these analyses, we investigated several types of anions (Figure 1e), among which the ClO_4^- exhibits the highest nucleophilicity with a small size.[31] Additionally, the relatively more negative electrostatic potential (ESP) of the core Cl atom in ClO_4^- highlights the great potential of ClO_4^- as a stabilizer for positive-valence S (Figure 1f).[32]

We then fabricated Zn||S cells using $ZnSO_4$, $Zn(TFSI)_2$, $Zn(OTF)_2$, $ZnCl_2$, and $Zn(ClO_4)_2$ as electrolytes in the hope of activating sulfur oxidation. All electrolytes were prepared at saturated concentrations to provide sufficient anions for redox reactions of the sulfur cathode. To improve the conductivity of the sulfur cathode, commercial sulfur powders were encapsulated into carbon spheres (CSs), resulting in uniform S/CSs composites with spherical morphology and ≈48.9% S loading content (Figures S1 and S2, Supporting Information). As depicted in cyclic voltammetry (CV) curves (Figure 1g), Zn||S cells with $ZnSO_4$, $Zn(TFSI)_2$, $Zn(OTF)_2$, or $ZnCl_2$ electrolytes only present cathodic behavior below 0.5 V, corresponding to the S^0 to S^{2-} conversion.[15,33] In contrast, the cell with 8 M $Zn(ClO_4)_2$ electrolyte exhibits a distinct two-step conversion process, featuring two primary cathodic peaks at 1.42 and 0.63 V, which suggests potential multivalence conversion of sulfur cathode in the ClO_4^--containing electrolyte.[25,34] We further conducted a galvanostatic charge/discharge (GCD) test of the Zn||S cells. As shown in Figure 1h, the Zn||S cells using $ZnSO_4$, $Zn(TFSI)_2$, $Zn(OTF)_2$, or $ZnCl_2$ electrolyte display a single discharge plateau (≈0.27 V) with a discharge capacity below 900 mAh g^{-1} (all capacity is calculated based on the mass of active materials without specific illustrations), while the Zn||S cell with $Zn(ClO_4)_2$ electrolyte demonstrates two discharge plateaus (1.38 and 0.36 V) with an impressive discharge capacity up to 1284 mAh g^{-1}. To confirm sulfur oxidation in the $Zn(ClO_4)_2$-based Zn||S cell, we collected X-ray photoelectron spectra (XPS) of the sulfur cathode at the initial state and fully charged state (Figure 1i). According to S 2p XPS spectra, new peaks at 169.8 and 168.5 eV are detected at 2.1 V charging state, which are assigned to the S^{4+} product.[25,35] Also, an obvious signal of ClO_4^- can be detected in the electrode at 2.1 V charging state compared with the electrode at the initial state, indicating ClO_4^- coordinates with S^{4+} to stabilize the positive-valence product (Figure S3, Supporting Information). These results demonstrate successful sulfur oxidation in the $Zn(ClO_4)_2$-based Zn||S cell, representing significant progress with the highest discharge voltage ever achieved in Zn||S batteries.

2.2. Inhibition of Positive-Valence S Dissolution

Although sulfur oxidation is successfully achieved by employing $Zn(ClO_4)_2$ aqueous electrolyte, yellow sulfur products appear on separators after cycling (see the inset picture in **Figure 2a**), as evidenced by Raman spectrum and XRD pattern in Figures S4 and S5 (Supporting Information), indicating dissolution and decomposition of positive-valence S compounds in the aqueous electrolyte.[25] The conversion pathway is even changed after ten cycles, revealed by the disappearance of multiplateaus (Figure 2a). To suppress the dissolution and decomposition of positive-valence S compounds in water, we employed a SN–$Zn(ClO_4)_2$ eutectic electrolyte to substitute $Zn(ClO_4)_2$ aqueous electrolyte.[36] It is worth noting that the maximum ClO_4^- concentration in the eutectic electrolyte is around 2.5 times higher than that in aqueous electrolytes (Figure 2b), which is beneficial for stabilizing positive-valence S during cycling. The SN–$Zn(ClO_4)_2$ eutectic electrolytes (see the chemical structures in Figure 2c) were prepared with different molar ratios of SN and $Zn(ClO_4)_2$ ranging from 3:1 to 1:1, denoted as SZ-3:1, SZ-2:1, and SZ-1:1, respectively. As shown in Figure 2d, SZ-3:1 and SZ-2:1 exhibit a homogeneous liquid state, while SZ-1:1 turns into an opaque solid-like state, indicating immiscibility of SN and $Zn(ClO_4)_2$ at this ratio. Obvious characteristic peaks of C—C≡N, C—C—C, and —C≡N in SN are observed in SZ-3:1 and SZ-2:1, which verifies the stable mixture of SN and $Zn(ClO_4)_2$ (Figure 2e; Figure S6, Supporting Information). However, these peaks are absent in SZ-1:1, likely due to formation of rigid crystal structures.[37,38] Besides, the free anion ratio of SZ-2:1 reaches an optimal value of 72%, with an excellent ionic conductivity of 1.56 $\times 10^{-3}$ S cm^{-1} (Figure 2f).

Zn||S cells were subsequently fabricated to investigate electrochemical performance of the designed eutectic electrolytes. The SZ-2:1 cell displays a multistep conversion process, with three distinct cathodic peaks at 1.54, 1.21, and 0.18 V (Figure 2g). Correspondingly, as depicted in GCD curves, the SZ-2:1 cell exhibits three discharge plateaus at 1.54, 1.24, and 0.26 V, and achieves a discharge capacity of up to 572 mAh g^{-1}, a significant improvement over SZ-3:1 and SZ-1:1 cell (Figure 2h). The higher discharge voltage indicates an enhanced positive-valence S conversion reaction in the eutectic electrolyte, likely attributed to superior compatibility between S cathode and eutectic electrolyte compared to the aqueous systems.[39,40] Furthermore, the low interface resistance confirms fast ion transport (Figure S7, Supporting Information), which can facilitate conversion reactions during cycling. In addition, we also increased the loading mass of sulfur active materials to investigate the electrochemical performance further (Figure S8, Supporting Information). The as-fabricated cell exhibits the simultaneous three discharge plateaus at 1.41, 1.21, and 0.19 V, and achieves a discharge capacity of 464 mAh g^{-1}, which is far below the electrode with 2 mg cm^{-2} loading mass. However, it is worth noting that the achieved capacity is far below the theoretical capacity of the sulfur electrode undergoing the six-electron transfer process. This can be attributed to the poor conductivity and low reversibility of sulfur and corresponding products.[25] These results demonstrate significantly enhanced S conversion activity by using the eutectic electrolyte. Most importantly, dissolution of positive-valence S compounds during cycling is successfully suppressed (Figure S9, Supporting Information), demonstrating superiority of the SN-based eutectic electrolyte over $Zn(ClO_4)_2$ aqueous electrolyte.

2.3. Reaction Pathways of Multivalent S Conversion

To unveil conversion mechanism of S cathode in the eutectic electrolyte-based Zn||S cell, we first examined ex situ XPS spectra of S cathode at different charging/discharging states

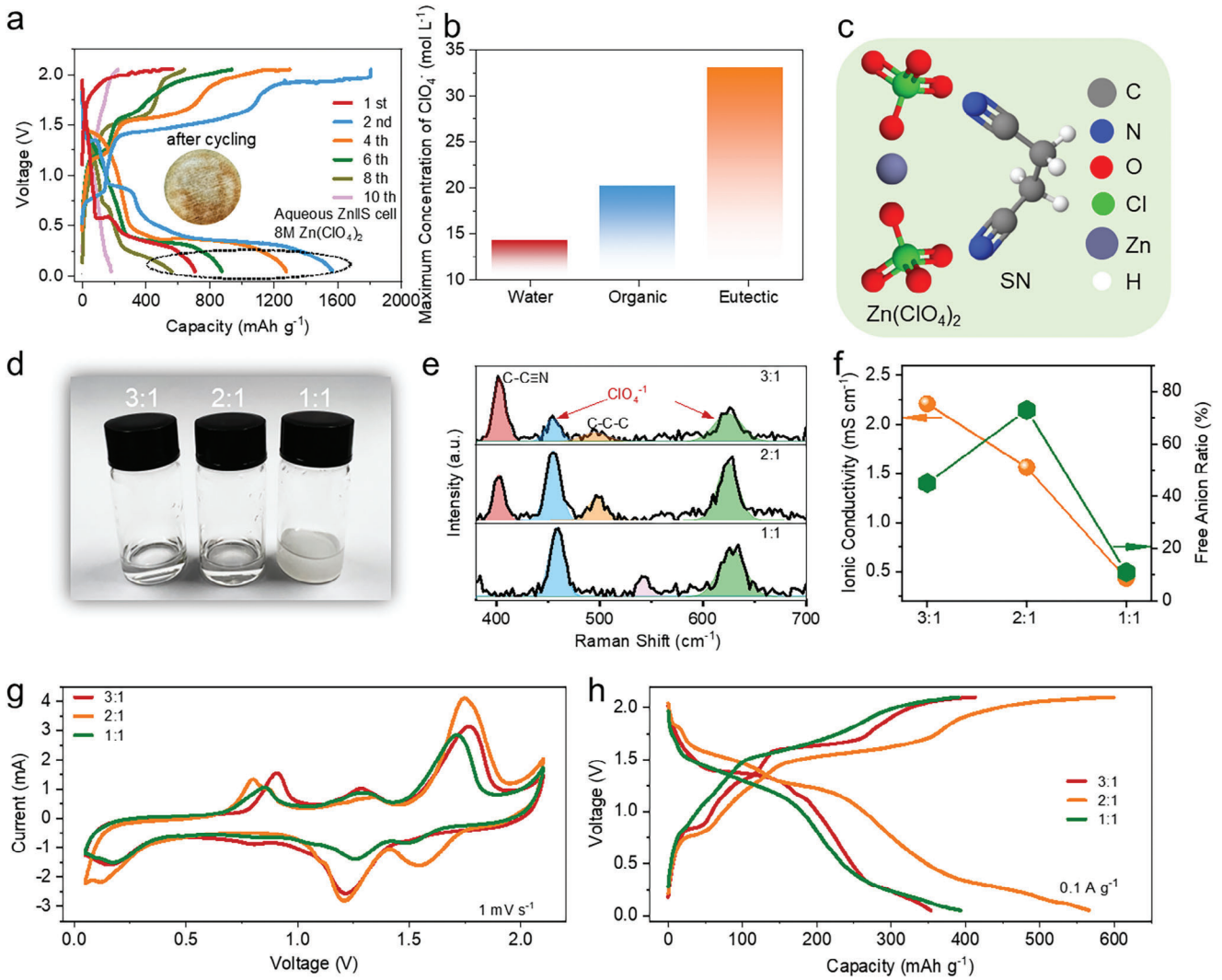

Figure 2. Electrolyte optimization for Zn||S cells. a) GCD curves of the Zn||S cell with 8 M $Zn(ClO_4)_2$ aqueous electrolyte at 0.1 A g^{-1} (inset picture: optical picture of the separator after cycling for ten cycles). b) Maximum ClO_4^- concentration in different electrolyte systems. c) Chemical structures of $Zn(ClO_4)_2$ and SN. d) Optical pictures, e) Raman spectra, and f) ionic conductivity, and free anion ratio of the eutectic electrolytes. g) CV curves and h) GCD curves of the Zn||S cells with eutectic electrolytes.

(**Figure** 3a–c). In addition to S^0 characteristic peaks in S 2p XPS spectra, new peaks appear at higher and lower binding energies during charging/discharging, suggesting a multivalence conversion of S cathode. We fitted these characteristic peaks to analyze valence evolution of S at different states (Figure 3c). At initial state (point A), the two peaks at 165.3 and 164.2 eV are assigned to S^0, while at 0.05 V discharging state (point G), the peaks shift to 163.4 and 162.1 eV, corresponding to S^{2-}, revealing the S reduction during discharging.[41] As the cell is charged back to 0.5 V (point H), disappearance of S^{2-} peaks and reemergence of S^0 peaks indicate reversible conversion from S^{2-} to S^0.[25,42] When the cell is charged to above 1.6 V (point J), new peaks at 169.8 and 168.5 eV corresponding to S^{4+} product are detected.[25] Thus, S cathode undergoes a six-electron transfer process with a multivalence conversion from S^{2-} to S^0 to S^{4+}. The reversible redox reaction of the S cathode is further confirmed by in situ Raman spectra (Figure 3d; Figure S10, Supporting Information). During the charging process, the intensity of peaks at 156.4, 226.1, and 475.8 cm^{-1} (assigned to S^0) gradually weakens, and a new peak at 530.3 cm^{-1} (assigned to $S(ClO_4)_3^+$) appears, indicating the conversion from S^0 to S^{4+}.[25,43,44] Additionally, XPS spectra of Cl 2p and Zn 2p (Figures S11 and S12, Supporting Information) at 2.1 V charging state show a strong ClO_4^- peak but no Zn 2p peak at S cathode, implying that ClO_4^- from the electrolyte potentially forms coordination with oxidized S.[12,45] By contrast, at 0.05 V discharging state, the ClO_4^- peak is diminished and Zn 2p peaks are detected at S cathode, likely relating to reversible reduction of S^{4+} to S^{2-} and generation of ZnS. In addition, the XRD patterns of the S cathodes at different charging/discharging states also confirm the proposed conversion mechanism, in which the ZnS discharging product can be clearly defined (Figure S13, Supporting Information).

In order to gain a comprehensive understanding of the electrochemical reaction pathways of the S cathode, we performed

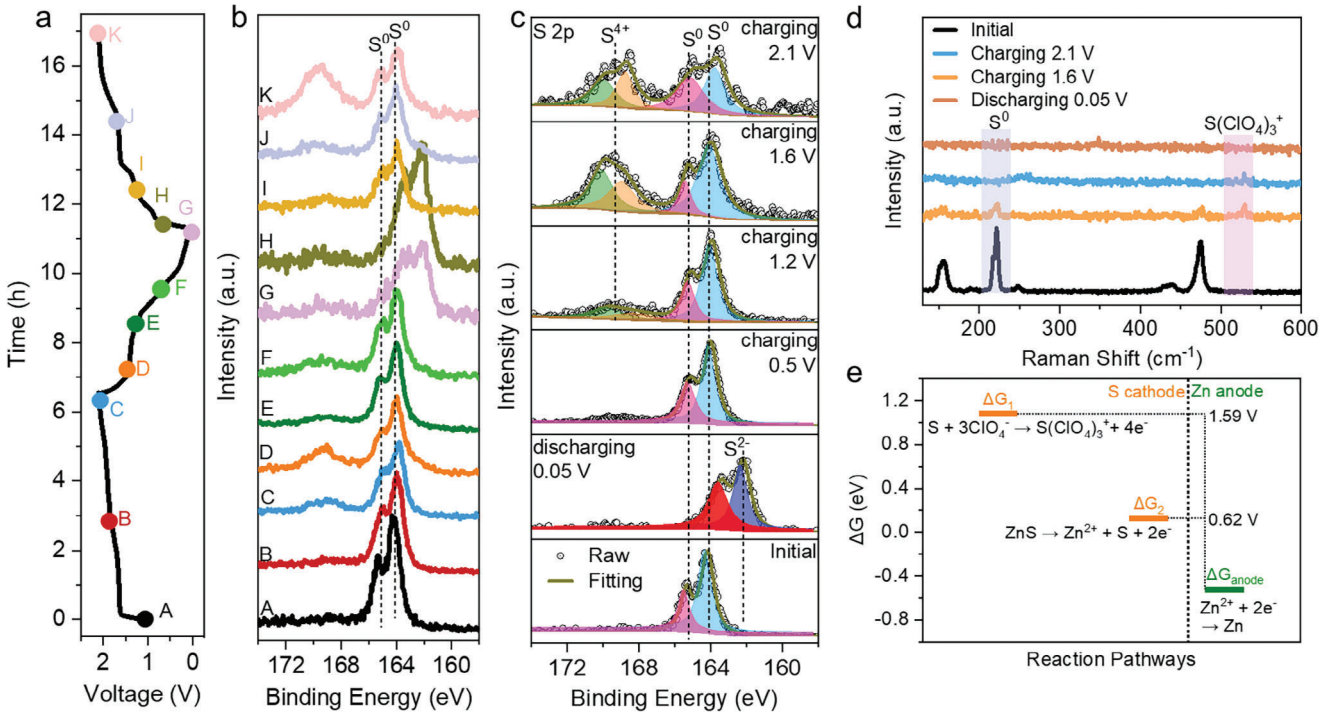

Figure 3. Investigations on conversion mechanism and reaction pathways. a) GCD curves of Zn||S cell at 0.1 A g^{-1} (the different color spheres indicate the potentials at which ex situ XPS spectra are collected. b) Ex situ XPS spectra at selected potentials. c) XPS fitting for S valence analysis. d) Raman patterns of S cathode at different charging/discharging states. e) Theoretical computations of reaction pathways of S redox process.

density functional theory (DFT) calculations to simulate interactions between S and the developed eutectic electrolyte. In general, S^{2-} favors the formation of stable ZnS in the presence of Zn^{2+}-containing electrolyte, and in the eutectic electrolyte, sufficient free ClO_4^- anions are potential to coordinate with positive-valence S.[15,36] Thus, we optimized the product structures and conducted calculations of Gibbs free energy. As shown in Figure 3e, the redox potential of S^{4+}/S^0 is calculated to be 1.59 V (vs Zn^{2+}/Zn), close to the experimental discharge plateau in Figure 2h.[25] The results further solidify the evidence for the six-electron transfer of S cathode facilitated by the eutectic electrolyte with high-nucleophilicity ClO_4^- anions. Based on the above experimental and theoretical analysis, we summarize the conversion reaction process of the Zn||S cell as follows

Cathode

$$\text{First step}: ZnS \leftrightarrow S + Zn^{2+} + 2e^- \quad (1)$$

$$\text{Second step}: S + 3ClO_4^- \leftrightarrow S(ClO_4)_3^+ + 4e^- \quad (2)$$

Anode

$$Zn^{2+} + 2e^- \leftrightarrow Zn \quad (3)$$

$$\text{Overall reaction}: ZnS + 2Zn^{2+} + 3ClO_4^- \leftrightarrow S(ClO_4)_3^+ + 3Zn \quad (4)$$

2.4. Zn||S Batteries Based on S Oxidation

We examined the electrochemical performance of the eutectic electrolyte-based Zn||S batteries. Despite the decent capacity and enhanced S redox activity with a six-electron transfer conversion, the battery undergoes capacity decay after ten cycles. It retains 50.8% of the initial capacity after 100 cycles (**Figure 4a**), probably due to the generation of inert ZnS. Thus, we adjusted the voltage window to 0.9–2.1 V to only allow for S^0/S^{4+} redox conversion and eliminate the generation of inert ZnS. As suggested by CV curves, S^0/S^{4+} redox reaction is achieved with good stability and gradually enhanced reaction activity (Figure S14, Supporting Information). The GCD curves highlight two discharge plateaus at 1.53 and 1.27 V with a discharge capacity of 304 mAh g^{-1} (Figure 4b). Notably, cycling stability is greatly improved, with a capacity retention of 87.8% after 100 cycles, indicating superior reversibility of S^0/S^{4+} redox conversion and excellent stability of S cathode during cycling.

Rate performance was further evaluated by GCD curves at different current densities (Figure 4c). The discharge plateaus remain stable across rates, delivering decent discharge capacities of 304, 253, 214, 179, 160, and 145 mAh g^{-1} at 0.1, 0.5, 1, 2, 3, and 4 A g^{-1}, respectively. The discharge capacity recovers to 282 mAh g^{-1} when the rate reverts to 0.1 A g^{-1} (Figure 4d), indicating a high tolerance of S cathode to fast conversion reactions. This outcome signifies the great advantage of conversion-type S cathodes over intercalation-type cathodes in fabricating reversible ZBs. Additionally, we compared energy density and power density of our high-voltage Zn||S battery with those of other ZBs in Figure 4e.[9,46–57] Remarkably, benefiting from the multivalence S conversion and flat discharge plateaus, our high-voltage Zn||S battery delivers significantly higher energy density (527 Wh kg_S^{-1} for S^{2-}/S^{4+} conversion and 410 Wh kg_S^{-1} for S^0/S^{4+} conversion) and power density

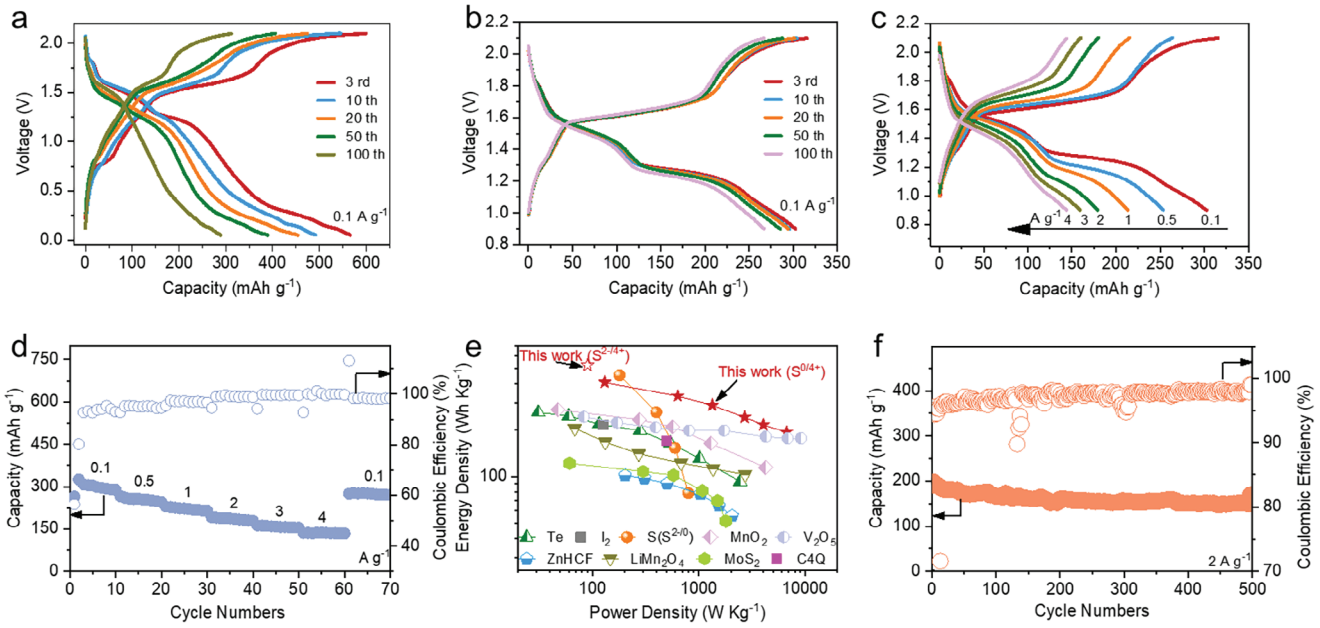

Figure 4. Electrochemical performance of the eutectic electrolyte-based Zn||S battery. a) GCD curves within 0.05–2.1 V. b) GCD curves of the Zn||S battery within 0.9–2.1 V. c) GCD curves at different densities and d) the corresponding rate performance. e) Ragone plot of our Zn||S battery and other reports. f) long-term cycling performance of the developed Zn||S battery.

(5612 W kg $_S^{-1}$) than other reported ZBs (Figure 4e; Figure S15, Supporting Information).[9,46–57] Moreover, the long-term cycling stability test at 2 A g^{-1} reveals a retained capacity of 169 mAh g^{-1} after 500 cycles, demonstrating an impressive capacity retention of 85.7% with a Coulombic efficiency (CE) of 98.4% (Figure 4f). These results are considerably superior to those of other metal–sulfur batteries based on multivalence S conversion, as indicated in Figure S16 and Table S1 (Supporting Information).[25,34,58,59] Such good performance stems from the highly reversible S redox conversion by virtue of suppressed positive-valence S compound dissolution (Figure S9, Supporting Information). It is worth noting that this Zn||S battery is fabricated at a far lower cost, surpassing conventional energy storage devices (Figure S17, Supporting Information). Therefore, our Zn||S battery, which exhibits high voltage, high energy density, and low cost, showcases its immense potential for practical applications.

2.5. Conversion Kinetics of S Oxidation

We adopted the polarization measurement to disclose conversion kinetics of the fabricated Zn||S battery. As shown in dQ/dV versus capacity plots (**Figure** 5a), the Zn||S battery with S^0/S^{4+} redox conversion displays an extremely low polarization voltage of 0.31 V compared to the battery with S^{2-}/S^0 redox conversion (showing a polarization voltage of 1.24 V). With CV scanning rate increasing from 1.0 to 2.5 mV s^{-1}; the minimal peak shift (Figure 5b) confirms fast conversion kinetics of S cathode during charging/discharging. Additionally, the slopes of cathodic peaks (0.66, 0.83) and anodic peaks (0.85, 0.57) (Figure 5c) suggest that the reactions are primarily diffusion-controlled rather than capacitive, further implying intrinsic fast conversion kinetics of S cathode.[60] The excellent conductivity of S/CSs composites with large contact area between active materials and electrolytes also facilitates the conversion kinetics.[61]

Galvanostatic intermittent titration technique (GITT) provides further insights into the cathode voltage response (Figure 5d).[62] The total overvoltage in region 1 ($S^{4+/0}$ plateau region) is 71 mV, much lower than that in region 2 (182 mV).[62] The higher overvoltage in region 2 is attributed to larger voltage jump and slower ion diffusion accompanying the typical phase transition, indicating the formation of different compounds in these two stages, consistent with the proposed conversion reaction mechanism. Furthermore, compared to the low ion diffusivity in S^0/S^{2-} plateau region (1.26×10^{-10}), faster ion diffusivity (4.79×10^{-9} cm^2 s^{-1}) is attained in S^{4+}/S^0 plateau region (Figure 5e). Such a high ion diffusion coefficient indicates superior sulfur oxidation kinetics in our Zn||S battery over sulfur reduction kinetics in traditional Zn||S batteries.[15]

3. Conclusion

Positive-valence conversion of sulfur is highly promising for constructing high-voltage Zn||S batteries; however, electrochemical oxidation of sulfur cathode has not been successful in Zn||S batteries due to instability of S^{n+} compound and formation of inert ZnS product. In this study, we achieved multivalence S conversion in Zn||S batteries by using a $Zn(ClO_4)_2$ electrolyte and the activated reaction pathways (S^{2-} to S^0 to S^{4+}) were well confirmed by spectroscopic analysis and theoretical computations. The optimal eutectic electrolyte further stabilized positive-valence S compound, resulting in excellent reversibility. The flat discharge plateaus arising from S^{4+}/S^0 demonstrated the highest operation voltage (1.54 V) achieved to date in Zn||S batteries. Remarkable rate performance, outstanding cycling performance, and exceptional energy density were also achieved in our

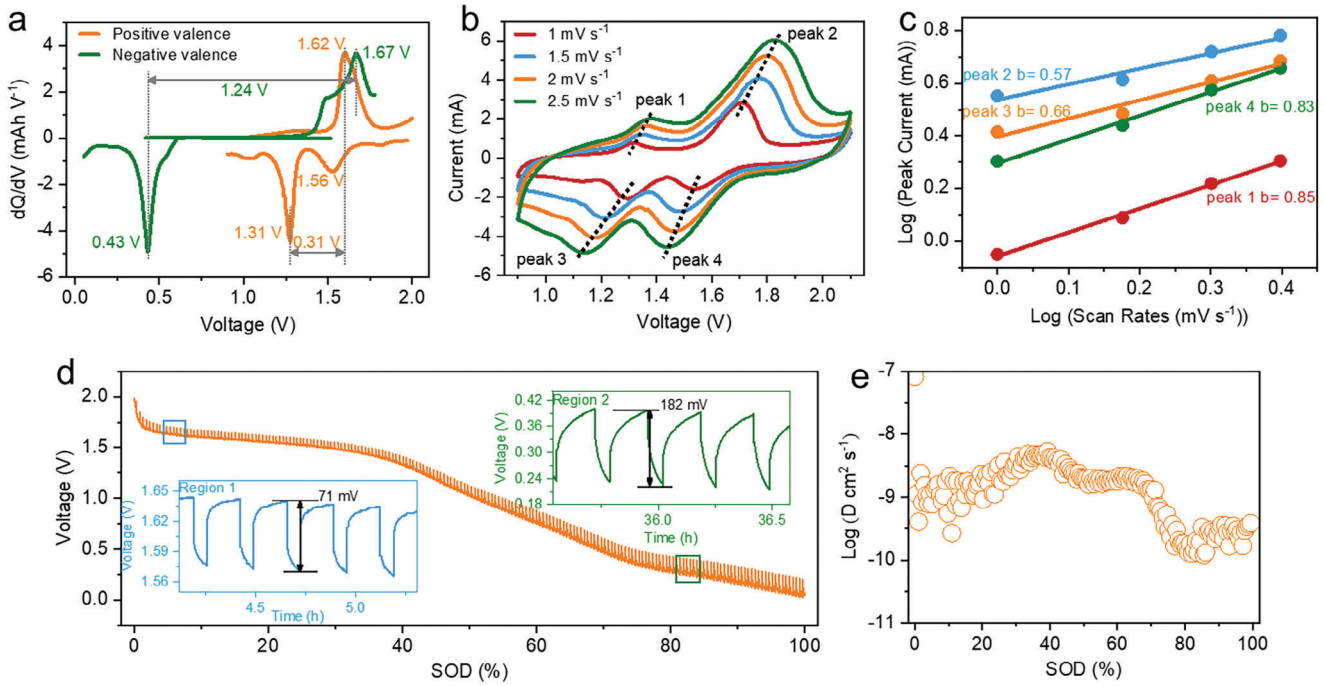

Figure 5. Investigations on conversion kinetics of the eutectic electrolyte-based Zn||S battery. a) dQ/dV versus capacity plot of discharge–charge profile of the Zn||S battery at 0.1 A g^{-1}. b) CV curves with scan rates ranging from 1.0 to 2.5 mV s^{-1}. c) The relationship between log (peak current) and log (scan rate). d) GITT profiles of the Zn||S battery (0.1 A g^{-1} for 60 s followed by a 30 min rest). e) Ion diffusion coefficient in S cathode.

high-voltage Zn||S battery. We expect that this electrolyte design approach to enhance multivalence S conversion activity can be coupled with a variety of metal anodes for fabricating high-energy and reversible sulfur-based batteries.

Received: February 26, 2024
Revised: June 5, 2024
Published online: June 17, 2024

Supporting Information

Supporting Information is available from the Wiley Online Library or from the author.

Acknowledgements

Z.C. and Z.H. contributed equally to this work. The work described in this paper was supported by a grant from the Research Grants Council of the Hong Kong Special Administrative Region, China (Project No. CityU C1002-21G). This work was also partially supported by a grant from Shenzhen Science and Technology Program (Program No. SGDX20211123151002003) and Innovation and Technology Fund (Grant No. GHP/191/21SZ).

Conflict of Interest

The authors declare no conflict of interest.

Data Availability Statement

The data that support the findings of this study are available from the corresponding author upon reasonable request.

Keywords

conversion-type cathode, eutectic electrolytes, positive-valence conversion of sulfur, sulfur cathode, zinc batteries

[1] J. M. Tarascon, M. Armand, *Nature* **2001**, *414*, 359.
[2] Y. Liang, H. Dong, D. Aurbach, Y. Yao, *Nat. Energy* **2020**, *5*, 646.
[3] J. Ming, J. Guo, C. Xia, W. Wang, H. N. Alshareef, *Mater. Sci. Eng., R* **2019**, *135*, 58.
[4] T. Zhang, Y. Tang, S. Guo, X. Cao, A. Pan, G. Fang, J. Zhou, S. Liang, *Energy Environ. Sci.* **2020**, *13*, 4625.
[5] B. Tang, L. Shan, S. Liang, J. Zhou, *Energy Environ. Sci.* **2019**, *12*, 3288.
[6] J. Shin, J. Lee, Y. Park, J. W. Choi, *Chem. Sci.* **2020**, *11*, 2028.
[7] C. Xu, B. Li, H. Du, F. Kang, *Angew. Chem., Int. Ed.* **2012**, *51*, 933.
[8] Q. Li, K. Ma, C. Hong, Z. Yang, C. Qi, G. Yang, C. Wang, *Energy Storage Mater.* **2021**, *42*, 715.
[9] N. Zhang, Y. Dong, M. Jia, X. Bian, Y. Wang, M. Qiu, J. Xu, Y. Liu, L. Jiao, F. Cheng, *ACS Energy Lett.* **2018**, *3*, 1366.
[10] B. Yong, D. Ma, Y. Wang, H. Mi, C. He, P. Zhang, *Adv. Energy Mater.* **2020**, *10*, 2002354.
[11] Q. Yang, X. Li, Z. Chen, Z. Huang, C. Zhi, *Acc. Mater. Res.* **2022**, *3*, 78.
[12] Z. Chen, C. Li, Q. Yang, D. Wang, X. Li, Z. Huang, G. Liang, A. Chen, C. Zhi, *Adv. Mater.* **2021**, *33*, 2105426.
[13] C. Feng, X. Jiang, Q. Zhou, T. Li, Y. Zhao, Z. Niu, Y. Wu, H. Zhou, M. Wang, X. Zhang, M. Chen, L. Ni, G. Diao, Y. Wei, *J. Mater. Chem. A* **2023**, *11*, 18029.
[14] L. Ni, J. Gu, X. Jiang, H. Xu, Z. Wu, Y. Wu, Y. Liu, J. Xie, Y. Wei, G. Diao, *Angew. Chem., Int. Ed.* **2023**, *62*, 202306528.
[15] W. Li, K. Wang, K. Jiang, *Adv. Sci.* **2020**, *7*, 2000761.
[16] J. F. Blais, Z. Djedidi, R. B. Cheikh, R. D. Tyagi, G. Mercier, *Pract. Period. Hazard., Toxic, Radioact. Waste Manage.* **2008**, *12*, 135.

[17] W. Zhang, M. Wang, J. Ma, H. Zhang, L. Fu, B. Song, S. Lu, K. Lu, *Adv. Funct. Mater.* **2022**, *33*, 2210899.
[18] S. Zhang, R. Liu, C. Streb, G. Zhang, *Polyoxometalates* **2023**, *2*, 9140037.
[19] D. Liu, B. He, Y. Zhong, J. Chen, L. Yuan, Z. Li, Y. Huang, *Nano Energy* **2022**, *101*, 107474.
[20] M. Yang, Z. Yan, J. Xiao, W. Xin, L. Zhang, H. Peng, Y. Geng, J. Li, Y. Wang, L. Liu, Z. Zhu, *Angew. Chem., Int. Ed.* **2022**, *61*, 202212666.
[21] X. F. Zhang, S. Q. Jiao, J. Tu, W. L. Song, X. Xiao, S. Li, M. Y. Wang, H. P. Lei, D. H. Tian, H. S. Chen, D. N. Fang, *Energy Environ. Sci.* **2019**, *12*, 1918.
[22] Z. Chen, H. Cui, Y. Hou, X. Wang, X. Jin, A. Chen, Q. Yang, D. Wang, Z. Huang, C. Zhi, *Chem* **2022**, *8*, 2204.
[23] D. Zang, H. Wang, *Polyoxometalates* **2022**, *1*, 9140006.
[24] S. G. Bratsch, *J. Phys. Chem. Ref. Data* **1989**, *18*, 1.
[25] H. Li, R. Meng, Y. Guo, B. Chen, Y. Jiao, C. Ye, Y. Long, A. Tadich, Q.-H. Yang, M. Jaroniec, S.-Z. Qiao, *Nat. Commun.* **2021**, *12*, 5714.
[26] Z. Chen, F. Mo, T. Wang, Q. Yang, Z. Huang, D. Wang, G. Liang, A. Chen, Q. Li, Y. Guo, X. Li, J. Fan, C. Zhi, *Energy Environ. Sci.* **2021**, *14*, 2441.
[27] D. Zang, X. J. Gao, L. Li, Y. Wei, H. Wang, *Nano Res.* **2022**, *15*, 8872.
[28] Z. Chen, S. Wang, Z. Wei, Y. Wang, Z. Wu, Y. Hou, J. Zhu, Y. Wang, G. Liang, Z. Huang, A. Chen, D. Wang, C. Zhi, *J. Am. Chem. Soc.* **2023**, *145*, 20521.
[29] T. Zhou, H. Wan, M. Liu, Q. Wu, Z. Fan, Y. Zhu, *Mater. Today Energy* **2022**, *27*, 101025.
[30] Z. Huang, Y. Hou, T. Wang, Y. Zhao, G. Liang, X. Li, Y. Guo, Q. Yang, Z. Chen, Q. Li, L. Ma, J. Fan, C. Zhi, *Nat. Commun.* **2021**, *12*, 3106.
[31] W. Zhang, Y. Lu, L. Wan, P. Zhou, Y. Xia, S. Yan, X. Chen, H. Zhou, H. Dong, K. Liu, *Nat. Commun.* **2022**, *13*, 2029.
[32] B. Khalili, M. Mamaghani, N. Bazdid-Vahdati, *Theor. Chem. Acc.* **2022**, *141*, 3.
[33] D. Zang, Q. Li, G. Dai, M. Zeng, Y. Huang, Y. Wei, *Appl. Catal., B* **2021**, *281*, 119426.
[34] G. Mamantov, J. Hvistendahl, *J. Electroanal. Chem. Interfacial Electrochem.* **1984**, *168*, 451.
[35] S. Wei, S. Xu, A. Agrawral, S. Choudhury, Y. Lu, Z. Tu, L. Ma, L. A. Archer, *Nat. Commun.* **2016**, *7*, 11722.
[36] C. Zhang, L. Zhang, G. Yu, *Acc. Chem. Res.* **2020**, *53*, 1648.
[37] J. Wang, Z. Zhao, G. Lu, Y. Zhang, Q. Kong, J. Zhao, G. Cui, *Mater. Today Energy* **2021**, *20*, 100630.
[38] W. Yang, X. Du, J. Zhao, Z. Chen, J. Li, J. Xie, Y. Zhang, Z. Cui, Q. Kong, Z. Zhao, *Joule* **2020**, *4*, 1557.
[39] W. Chu, X. Zhang, J. Wang, S. Zhao, S. Liu, H. Yu, *Energy Storage Mater.* **2019**, *22*, 418.
[40] Y. Liu, Y. Elias, J. Meng, D. Aurbach, R. Zou, D. Xia, Q. Pang, *Joule* **2021**, *5*, 2323.
[41] G. Chang, J. Liu, Y. Hao, C. Huang, Y. Yang, Y. Qian, X. Chen, Q. Tang, A. Hu, *Chem. Eng. J.* **2023**, *457*, 141083.
[42] M. Angell, C.-J. Pan, Y. Rong, C. Yuan, M.-C. Lin, B.-J. Hwang, H. Dai, *Proc. Natl. Acad. Sci. USA* **2017**, *114*, 834.
[43] A. T. Ward, *J. Phys. Chem.* **1968**, *72*, 4133.
[44] Y. Cheng, C. Jin, F. Gao, X. Wu, W. Zhong, S. Li, P. K. Chu, *J. Appl. Phys.* **2009**, *106*, 123505.
[45] Y.-C. Lin, Y.-Y. Chen, B.-Y. Yu, W.-C. Lin, C.-H. Kuo, J.-J. Shyue, *Analyst* **2009**, *134*, 945.
[46] Z. X. Liu, Q. Yang, D. H. Wang, G. J. Liang, Y. H. Zhu, F. N. Mo, Z. D. Huang, X. L. Li, L. T. Ma, T. C. Tang, Z. G. Lu, C. Y. Zhi, *Adv. Energy Mater.* **2019**, *9*, 1902473.
[47] L. Ma, S. Chen, H. Li, Z. Ruan, Z. Tang, Z. Liu, Z. Wang, Y. Huang, Z. Pei, J. A. Zapien, C. Zhi, *Energy Environ. Sci.* **2018**, *11*, 2521.
[48] G. J. Liang, F. N. Mo, D. H. Wang, X. L. Li, Z. D. Huang, H. F. Li, C. Y. Zhi, *Energy Storage Mater.* **2020**, *25*, 86.
[49] D. Wang, Y. Zhao, G. Liang, F. Mo, H. Li, Z. Huang, X. Li, T. Tang, B. Dong, C. Zhi, *Nano Energy* **2020**, *71*, 104583.
[50] H. L. Pan, B. Li, D. H. Mei, Z. M. Nie, Y. Y. Shao, G. S. Li, X. S. Li, K. S. Han, K. T. Mueller, V. Sprenkle, J. Liu, *ACS Energy Lett.* **2017**, *2*, 2674.
[51] D. H. Wang, L. F. Wang, G. J. Liang, H. F. Li, Z. X. Liu, Z. J. Tang, J. B. Liang, C. Y. Zhi, *ACS Nano* **2019**, *13*, 10643.
[52] Q. Zhao, W. Huang, Z. Luo, L. Liu, Y. Lu, Y. Li, L. Li, J. Hu, H. Ma, J. Chen, *Sci. Adv.* **2018**, *4*, eaao1761.
[53] K. Ghanbari, M. F. Mousavi, M. Shamsipur, H. Karami, *J. Power Sources* **2007**, *170*, 513.
[54] G. Yuan, J. Bai, T. N. L. Doan, P. Chen, *Mater. Lett.* **2014**, *137*, 311.
[55] P. He, Y. Quan, X. Xu, M. Yan, W. Yang, Q. An, L. He, L. Mai, *Small* **2017**, *13*, 1702551.
[56] L. Zhang, L. Chen, X. Zhou, Z. Liu, *Adv. Energy Mater.* **2015**, *5*, 1400930.
[57] H. Li, Q. Yang, F. Mo, G. Liang, Z. Liu, Z. Tang, L. Ma, J. Liu, Z. Shi, C. Zhi, *Energy Storage Mater.* **2019**, *19*, 94.
[58] M. E. Speer, M. Kolek, J. J. Jassoy, J. Heine, M. Winter, P. M. Bieker, B. Esser, *Chem. Commun.* **2015**, *51*, 15261.
[59] G. Cohn, L. Ma, L. A. Archer, *J. Power Sources* **2015**, *283*, 416.
[60] Z. Chen, Q. Yang, F. Mo, N. Li, G. Liang, X. Li, Z. Huang, D. Wang, W. Huang, J. Fan, *Adv. Mater.* **2020**, *32*, 2001469.
[61] Z. Chen, Q. Yang, D. Wang, A. Chen, X. Li, Z. Huang, G. Liang, Y. Wang, C. Zhi, *ACS Nano* **2022**, *16*, 5349.
[62] W. Sun, F. Wang, S. Hou, C. Yang, X. Fan, Z. Ma, T. Gao, F. Han, R. Hu, M. Zhu, C. Wang, *J. Am. Chem. Soc.* **2017**, *139*, 9775.